Spatial Lymphocyte Dynamics in Lymph Nodes Predicts the Cytotoxic T cell Frequency Needed for HIV Infection Control

1 Dmitry Grebennikov[1,2,3*], Anass Bouchnita[4], Vitaly Volpert[3,5,6], Nikolay
2 Bessonov[7], Andreas Meyerhans[8,9], Gennady Bocharov[2,10*]

3 [1]Moscow Institute of Physics and Technology (National Research University),
4 Dolgoprudny, Moscow Region, Russia

5 [2]Marchuk Institute of Numerical Mathematics, Russian Academy of Sciences,
6 Moscow, Russia

7 [3]Peoples' Friendship University of Russia (RUDN University), Moscow, Russia

8 [4]Division of Scientific Computing, Department of Information Technology, Uppsala
9 University, Uppsala, Sweden

10 [5]Institut Camille Jordan, UMR 5208 CNRS, University Lyon 1, Villeurbanne, France

11 [6]INRIA Team Dracula, INRIA Lyon La Doua, Villeurbanne, France

12 [7]Institute of Problems of Mechanical Engineering, Russian Academy of Sciences,
13 Saint Petersburg, Russia

14 [8]Infection Biology Laboratory, Department of Experimental and Health Sciences,
15 Universitat Pompeu Fabra, Barcelona, Spain

16 [9]Institució Catalana de Recerca i Estudis Avançats (ICREA), Barcelona, Spain

17 [10]Sechenov First Moscow State Medical University, Moscow, Russia

18 *** Correspondence:**

19 Dmitry Grebennikov, dmitry.ew@gmail.com

20 Gennady Bocharov, bocharov@m.inm.ras.ru

Supplementary Material

Supplementary Text

We estimated the numbers for immune cell subsets, i.e. DCs, CD4^{+} T cells and CD8^{+} T cells, in lymph nodes based on the data from (Kitano et al., 2016). First, the numbers of DCs were estimated by rescaling the whole LN flow cytometry counts to a computational domain. We assume that flow cytometry reveals about 10% of the total cellularity (Mario Novkovic, personal communication) and that the computational domain represents a central section of a bean-shaped LN of 10 μm depth. The semi-axes of the spheroid LN representation are $a = \frac{1}{2}1000\mu m$, $c = \frac{1}{2}600\mu m$, leading to the following values of the volumes of a LN: $V_{\text{LN}} = \frac{4\pi}{3}a^2 c \approx 0.3 \times 10^9 \mu m^3$, and the slice: $V_{\text{Slice}} = \pi ac \cdot z_{\text{depth}} \approx 4.7 \times 10^6 \mu m^3$. We note that rescaling the cell counts from (Kitano et al., 2016) using the assumptions stated above resulted in a biologically realistic dense packing of the computational domain ($\eta \approx 80\%$).

Given that the total protein mass per APC is in the range between 64 ± 14 pg and 95 ± 25 pg (for different dendritic cell subtypes) (Wiśniewski et al., 2014), and the estimation that the fraction of dry solids in a cell constitutes about 27% of the total mass (Brown, 1991, Illmer et al., 1999), we set the mass of wet APC to be 350 pg. The same approach was used to define the T cell mass. To estimate the T cell mass, we used lymphocyte wet weight measurements from (Segel et al., 1981). The here chosen value of 215 pg corresponds to a protein mass of 60 pg, which is in the range of the total protein mass of CD4^{+} T cells (Wiśniewski et al., 2014). As the protein mass of CD8^{+} T cells is on average 1.35 times larger than the protein mass of CD4^{+} T cells (Wiśniewski et al., 2014), we set the mass of wet CD8^{+} T cells to be 290 pg.

The T cell radius was set to 3 μm (Turgeon, 2005). APC diameter estimates vary from 7 to 15 μm (Wiśniewski et al., 2014; Goya et al., 2008). Most likely, the range is so wide because of different dendritic cell subtypes analyzed in references, and also because a dendritic cell represents a spherical body with numerous dendrites around. In our model, we define APCs as spherical circles with 13 μm diameter, which incorporates the area of dendrites, whereas we change the range of adhesive area in repulsion force to lie in (0.5r, r) ($\lambda_{DC} = 0.5$). Thus, the actual repulsive body of an APC is 6.5 μm, and the outer part $x \in (6.5, 13)$ μm is an adhesive dendritic area (see Figure 1C).

The adhesive strength between T cells, which is a weak nonspecific electrical force (Bell, 1978), is of the order of 0.01 to 0.03 nN (Basu and Huse, 2017, Kong et al., 2009). It was set to 0.01 nN. The specific adhesive strength between T cells and APCs is estimated to be around 1 nN, based on single cell force spectroscopy measurements (Lim et al., 2012). Also, from that publication, we roughly estimate the viscous

58 damping coefficient: the maximal force measured on the cantilever with a T cell
59 slowly approaching an APC was 1 nN, which leads to $\mu \approx 0.1\,nN \cdot min\,/\mu m$ if divided
60 by the typical lymphocyte velocity of 10 $\mu m/min$ (Miller et al., 2003). We tuned this
61 parameter to $\mu = 0.2 nN \cdot min/\mu m = 12\,g/s$ during calibration. The adhesive
62 strength between APCs is of the same value as the nonspecific adhesive strength
63 between T cells.

64 We set the motility magnitude to be sampled from $N(3, 0.3)$ nN distribution, so that
65 percentiles $P_1 \approx 2.3$ nN, $P_{99} \approx 3.7$ nN are positive and below the mechanical force of
66 ~ 5 nN, which is exerted by cytotoxic cells on target cells to potentiate their killing by
67 destructing their membrane (Basu et al., 2016). The mean and standard deviation were
68 also manually calibrated to ensure that the maximal cell velocity is <25µm/min and
69 that their overall profile matches a target cumulative distribution.

70 The standard deviation for the motility turning angle $\sigma(\alpha_{TC})$, the coefficient c_{inh} that
71 takes into account the level of CIL influence and the coefficient β parameterizing a
72 negative correlation between the motility magnitude and the turning angle, were set
73 according to the models they originate from (Read et al., 2016, Zimmermann et al.,
74 2016), and were tuned to match the T cell motility profile.

75 When performing *in silico* simulations to study the effect of decreased T cell motility
76 on target cell location efficiency (Figures 4D and 4E), the parameter η_i was used to
77 decrease the intrinsic motility. We evaluated that a 10% decrease of the average T cell
78 velocity from the baseline value corresponds to $\eta_i = 0.75$, the 50% decrease
79 corresponds to $\eta_i = 0.33$. To obtain statistics for Figure 4, N=400 realizations were
80 computed for each scenario of *in silico* simulations.

81 Visualization of the spatiotemporal dynamics of the multicellular system simulated
82 over a 3-hour period is presented in *Movie S1*.

Supplementary references:

84 1. Kitano M, Yamazaki C, Takumi A, Ikeno T, Hemmi H, Takahashi N, et al. Imaging
85 of the cross-presenting dendritic cell subsets in the skin-draining lymph node. *Proc.*
86 *Natl. Acad. Sci.* (2016) 113:1044–1049. doi: 10.1073/pnas.1513607113.

87 2. Wiśniewski JR, Hein MY, Cox J, Mann M. A "proteomic ruler" for protein copy
88 number and concentration estimation without spike-in standards. *Mol. Cell*
89 *Proteomics. MCP* (2014) 13:3497–3506. doi: 10.1074/mcp.M113.037309.

90 3. Brown GC. Total cell protein concentration as an evolutionary constraint on the
91 metabolic control distribution in cells. *J. Theor Biol.* (1991) 153:195–203. doi:
92 10.1016/S0022-5193(05)80422-9

93   4. Illmer P, Erlebach C, Schinner F. A practicable and accurate method to differentiate
94   between intra- and extracellular water of microbial cells. *FEMS Microbiol. Lett.* (1999)
95   178:135–139.

96   5. Segel GB, Cokelet GR, Lichtman MA. The measurement of lymphocyte volume:
97   importance of reference particle deformability and counting solution tonicity. *Blood*
98   (1981) 57:894–899.

99   6. Turgeon ML. *Clinical hematology: theory and procedures*. 4th ed. Philadelphia:
100   Lippincott Williams & Wilkins (2005).

101   7. Goya GF, Marcos-Campos I, Fernández-Pacheco R, Sáez B, Godino J, Asín L, et al.
102   Dendritic cell uptake of iron-based magnetic nanoparticles. *Cell. Biol Int.* (2008)
103   32:1001–1005. doi: 10.1016/j.cellbi.2008.04.001.

104   8. Bell GI. Models for the specific adhesion of cells to cells. *Science* (1978) 200:618–
105   627. doi: 10.1126/science.347575.

106   9. Basu R, Huse M. Mechanical communication at the immunological synapse. *Trends
107   Cell. Biol.* (2017) 27:241–254. doi: 10.1016/j.tcb.2016.10.005.

108   10. Kong F, García AJ, Mould AP, Humphries MJ, Zhu C. Demonstration of catch
109   bonds between an integrin and its ligand. *J. Cell Biol.* (2009) 185:1275–1284. doi:
110   10.1083/jcb.200810002.

111   11. Lim TS, Goh JKH, Mortellaro A, Lim CT, Hämmerling GJ, Ricciardi-Castagnoli
112   P. CD80 and CD86 differentially regulate mechanical interactions of T-cells with
113   antigen-presenting dendritic cells and B-cells. *PLOS ONE* (2012) 7:e45185. doi:
114   10.1371/journal.pone.0045185.

115   12. Miller MJ, Wei SH, Cahalan MD, Parker I. Autonomous T cell trafficking
116   examined *in vivo* with intravital two-photon microscopy. *Proc. Natl. Acad. Sci. USA*
117   (2003) 100:2604–2609. doi: 10.1073/pnas.2628040100.

118   13. Basu R, Whitlock BM, Husson J, Le Floc'h A, Jin W, Oyler-Yaniv A, et al.
119   Cytotoxic T cells use mechanical force to potentiate target cell killing. *Cell* (2016)
120   165:100–110. doi: 10.1016/j.cell.2016.01.021.

121   14. Read MN, Bailey J, Timmis J, Chtanova T. Leukocyte motility models assessed
122   through simulation and multi-objective optimization-based model selection. *PLOS
123   Comput. Biol.* (2016) 12:e1005082. doi: 10.1371/journal.pcbi.1005082.

124   15. Zimmermann J, Camley BA, Rappel W-J, Levine H. Contact inhibition of
125   locomotion determines cell–cell and cell–substrate forces in tissues. *Proc. Natl. Acad.
126   Sci. USA* (2016) 113:2660–2665. doi: 10.1073/pnas.1522330113.

Supplementary Movies

Legend for supporting video file "Movie_S1"

Visualization of the spatiotemporal dynamics of the multicellular system simulated over a 50 minutes period. The following cell subsets are considered: CD4$^+$ T cells, CD8$^+$ T cells and cross-presenting migratory CD8$^{\alpha int}$CD103^{hi} DCs. DCs, CD4$^+$ T cells and CD8$^+$ T cells are placed within a total cellularity of 12469 cells, 80% packing density and 1% precursor frequency. Both T cell subsets are distributed uniformly through the whole LN, while migratory DCs are found mainly deep in the paracortex area. The spatial positions for DC locations are iteratively sampled from the 2D Gaussian distribution with a 99-percentile ellipse DC and accepted if the DC with sampled coordinates lies within the LN domain and does not overlap with the other seeded DCs.
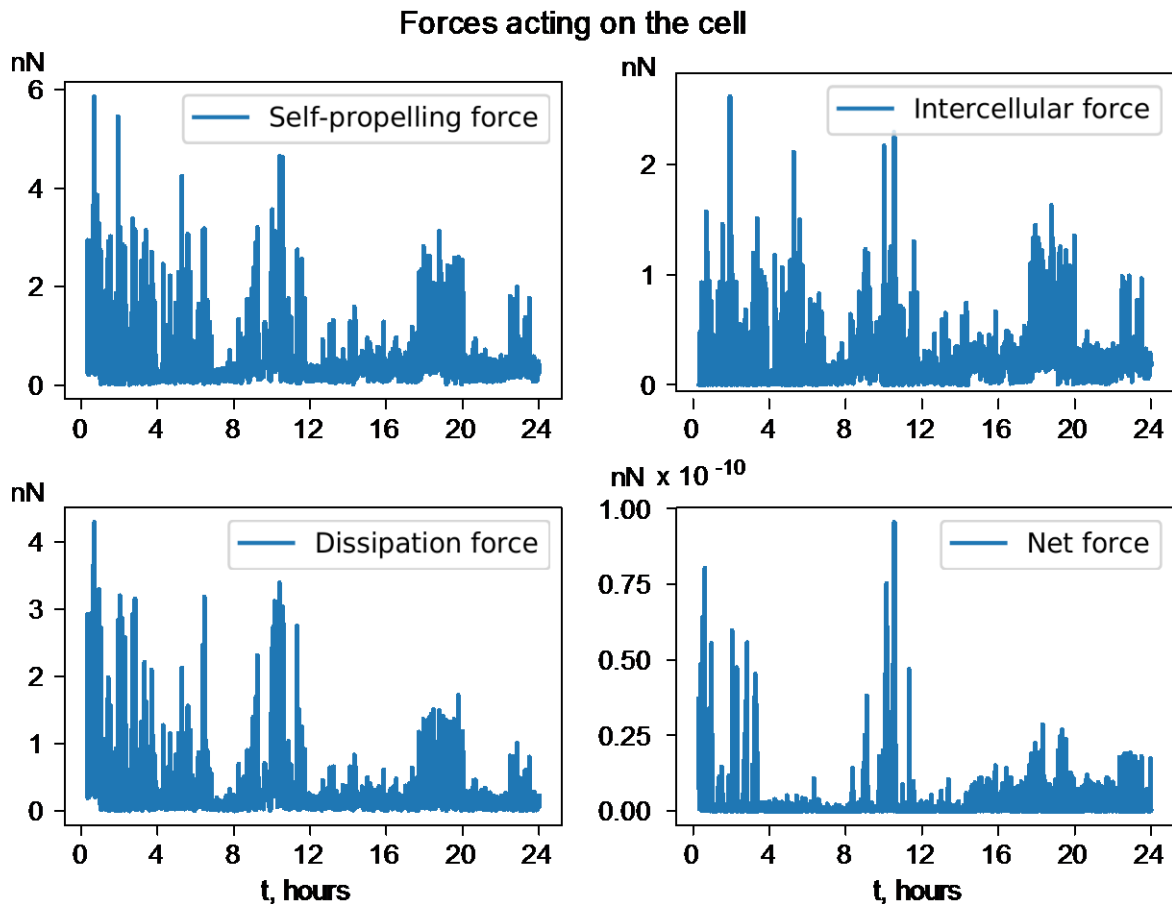
Supplementary Figures

Figure S1. The absolute values of the components of the net force acting on the randomly selected CD8$^+$ T cell in 24-hour of *in silico* simulations.